Applied Energy 150 (2015) 97–108

Contents lists available at ScienceDirect

Applied Energy

journal homepage: www.elsevier.com/locate/apenergy

An improved perturb and observe (P&O) maximum power point tracking (MPPT) algorithm for higher efficiency

Jubaer Ahmed, Zainal Salam *

Centre of Electrical Energy Systems, Faculty of Electrical Engineering, Universiti Teknologi Malaysia, 81310 Johor Bahru, Malaysia
Institute of Future Energy, Universiti Teknologi Malaysia, 81310 Johor Bahru, Malaysia

HIGHLIGHTS

- A improved P&O based MPPT method for PV system is developed.
- The method enhances the steady state performance of the conventional P&O.
- Proposed method minimizes the probability of losing the tracking direction.
- The energy yield is increased by 2% on average.
- No complex computation is required and hardware implementation is very simple.

ARTICLE INFO

Article history:
Received 19 August 2014
Received in revised form 31 March 2015
Accepted 5 April 2015
Available online 20 April 2015

Keywords:
Solar energy
Photovoltaic
P&O
MPPT
P–V curve
MPPT

ABSTRACT

This paper proposes a method to improve the efficiency of the P&O maximum power point tracker (MPPT) by reducing the steady state oscillation and eliminating the possibility of the algorithm to lose its tracking direction. A dynamic perturbation step-size is employed to reduce the oscillation, while boundary conditions are introduced to prevent it from diverging away from the MPP. To prove its effectiveness, the proposed P&O is compared with the conventional and adaptive P&O using the Ropp, sinusoidal and ramp irradiance tests. In addition, the performances are evaluated based on a one-day (10 h) irradiance and temperature profile. The algorithm is implemented on a buck-boost converter and benchmarked by the standard MPPT efficiency (η_{MPPT}) calculation. It was found that, for all the tests, the η_{MPPT} of the proposed P&O scheme is increased by approximately two percentage points. Besides, the proposed algorithm does not require any extra hardware components; only several lines of additional software codes are to be embedded into the conventional P&O MPPT control program.

1. Introduction

Solar photovoltaic (PV) is envisaged to be one of the key sources of the future energy mix. The cost of modules has declined sharply over the last decade and nowadays PV power plants with MW capacity are becoming a norm in many countries [1,2]. Despite this encouraging trend, the per-watt price of PV energy is still considerably expensive compared to its fossil fuel counterpart. The reason is clear; the capital investment of PV project (in terms of dollar per watt) is significantly higher than the latter. There are extensive research and development efforts to increase the PV energy throughput—mostly they are focused on improving the performance of the solar cell efficiency. However, this approach has its own constraint, primarily due to the physical limitations of silicon itself. Recently, new and more exotic semiconductor materials for PV cells are also being experimented [3,4], but the present cost of these technologies appears to be prohibitive. Consequently, they are mostly used in high-end products, for example for space application.

The more economical way to enhance the performance of the PV installation is to consider the balance of system (BOS) components, particularly the power converter (inverter or charger). One possible area of improvement is to increase the efficiency of the maximum power point tracking (MPPT) algorithm [5–7]. This is because the MPPT comprises only of software codes that can be embedded within the power converter firmware, i.e. without an additional cost. The MPPT automatically locates the maximum power point (MPP)—that is the desired operating voltage (V_{MPP}) or current (I_{MPP}) in order to achieve the maximum output power (P_{MPP}). Furthermore, the tracking must be dynamic, i.e. the

* Corresponding author. Tel.: +60 07 5536187; fax: +60 07 5566272.
E-mail addresses: jubaerahmed_eee@yahoo.com (J. Ahmed), zainals@fke.utm.my (Z. Salam).

http://dx.doi.org/10.1016/j.apenergy.2015.04.006
0306-2619/

operating point has to be continuously adjusted in response to the measured irradiance and temperature conditions. Thus locating the MPP is a complicated process because the environmental condition is constantly changing, while at the same time, the *P–V* curve itself exhibits non-linear characteristics.

Among the numerous MPPT techniques described in literature [8,9], the perturb and observe (P&O) [10,11] is the most popular. It is widely installed in commercial PV inverter using low cost microprocessors. Despite the simplicity and reliability of the algorithm, it inherently has two main drawbacks. First, when the tracking reaches the vicinity of the MPP, the operating point is forced to go back and forth around MPP, resulting in unending oscillation in the output power. As a result, the energy yield is reduced and hence a drop in the efficiency. Secondly, P&O is prone to lose its tracking direction, i.e. it could not cope with the change in the irradiance and causes the operating point to diverge away from the MPP locus. This divergence also results in energy loss.

This work is carried out to increase the efficiency the conventional P&O by simultaneously addressing both abovementioned problems. Structure-wise, of proposed algorithm is similar to the conventional MPP, but with two additional features: (1) it incorporates a dynamic built-in checking mechanism that guarantees the consistent detection of the oscillation and varies the perturbation size accordingly and (2) it establishes voltage boundaries to ensure that the operating point will not deviate from its tracking locus. It is acknowledged that there exist previous works to resolve the power oscillation by means of the adaptive P&O [10–18]. However, as shall be shown in this paper, the adaptive mechanism has a tendency to provoke the MPPT to go in the wrong direction and eventually causes the operating point to diverge from the MPP.

Another point to consider is that, for majority of the cases reported in literature, the MPPT algorithms are tested against simplistic irradiance profiles. In actuality, these tests do not reflect the conditions that occur in the real environment. Subsequently, the improvements in performance (as claimed) cannot be truly verified. Since there is a lack of benchmarking, this paper proposes a comprehensive evaluation of the proposed method, in comparison to the conventional and adaptive P&O. Three types of test, namely the Ropp [19], sinusoidal and ramp are used for this purpose. These tests are very stringent as it demands the MPPT to track the irradiance profiles of various shapes, gradient and duration very accurately. Furthermore, to understand how the proposed P&O performs under the real environmental condition, it is subjected to a one-day of continuous irradiance and the temperature variation.

The paper is organized as follows: after this introduction, a brief overview is given on the limitations of the conventional and adaptive P&O. These are well-known problems—thus for brevity, only a cursory information is given. In the next section, a detailed description on the proposed P&O is given. To prove the concept, a PV simulation based on two-diode model is explained. The type and specifications of module are also provided. A buck-boost experimental set-up to verify the effectiveness of the algorithm is described next. The three performance tests, as well as the daily profile as described above are carried out in the following section. The results are complemented by a comprehensive discussion.

2. Problems with the conventional P&O

2.1. Steady state oscillation near the MPP

In the conventional P&O, the power (P) is computed using the measured values of the voltage (V) and current (I) of the PV array. The algorithm provides a perturbation (ΔV) in V, based on the change of P by the following rule:

$$\begin{aligned} V_{new} &= V_{old} + \Delta V \times slope \quad (if\ P > P_{old}) \\ V_{new} &= V_{old} - \Delta V \times slope \quad (if\ P < P_{old}) \end{aligned} \tag{1}$$

In Eq. (1), the slope indicates the direction of the perturbation, i.e. to the right (climbing) or left (descending). The flowchart to implement P&O is given in Fig. 1(a). Clearly, the size of the perturbation, ΔV is crucial; if ΔV is large, the convergence is fast, but it results in large fluctuation in P, and vice versa. Whatever the case, algorithm will caused to operating point to continuously oscillate around the MPP, as depicted in Fig. 1(b). Obviously, the loss is more if the perturbation size is large. The oscillation is highly undesirable as it results is significant energy loss. That is why in the adaptive P&O is introduced [15,20].

2.2. Divergence from the tracking locus

Apart from the steady state loss, P&O is prone to diverge from its tracking locus, i.e. moving away from the MPP. This divergence usually happens when a gradual change of irradiance takes place [9]. As illustrated in Fig. 2, assume that in the beginning, P&O tracks the MPP at point A. Thus, the operating point oscillates around the MPP, i.e. moving back and forth between A, B and B′. Let's consider a case whereby while moving towards A, the irradiance starts to increase gradually. The operating point will reach at C instead of B. In this situation, the algorithm assumes the perturbation is in the direction of increasing power; thus it keeps on providing a perturbation in the same direction. As a result, the operating point is moves away from the MPP, i.e. following the path A-C-D-E, as shown in Fig. 2(a). Consequently, the operating point diverges from the MPP and will keep on doing so if the irradiance steadily increases. However it is necessary to note that, the loss of tracking direction only occurs when the irradiance increases gradually. When irradiance falls (both slow and faster rate), the same phenomena does not happen.

2.3. The adaptive P&O

The adaptive P&O algorithms can be based on the voltage [10,18,20,21] or duty cycle [13,22,23]. The adaptive mechanism intelligently varies the perturbation size to minimize steady state oscillation. When the operating point is far from the MPP, the perturbation is made larger. This is to ensure that the tracking speed is maximized. As the operating point gets closer the MPP, the perturbation size is dynamically reduced until it becomes very small. For example, in [21], the algorithm has an initial perturbation of 10% of V_{oc} but at steady state, its value is reduced to 0.5%.

There are various ways to vary the perturbation size. In [16], the following relationship is used:

$$\Delta V_{n+1} = M\frac{\Delta P_n}{\Delta V_n} \tag{2}$$

where ΔP and ΔV are the changes in power and voltage, respectively, while M is a constant that requires tuning. In another approach, [18] the perturbation size is determined as the logarithmic function as follows.

$$\Delta V_{n+1} = M\log_{10}\left(\frac{\Delta P_n}{\Delta V_n}\right) \tag{3}$$

The adaptive process is somewhat improved due to the logarithmic nature of the equation.

3. The proposed P&O

3.1. Outline of the scheme

The proposed scheme is designed to improve the performance of the P&O by removing the steady state oscillation and preventing

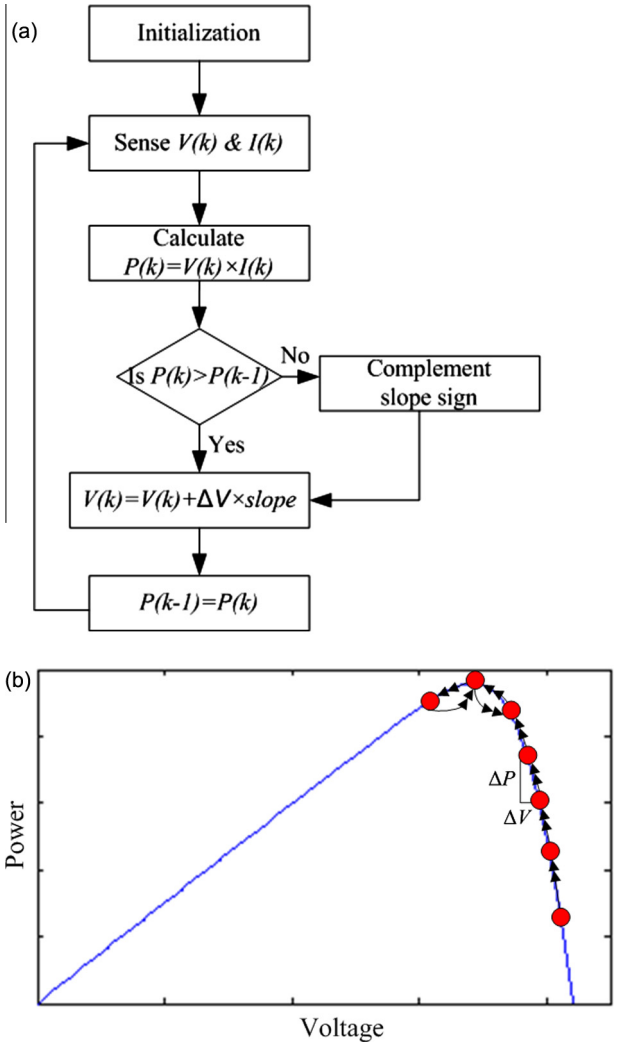

Fig. 1. (a) The basic flowchart of the conventional P&O, (b) the occurrence of oscillation of P&O around the steady state MPP.

the divergence of the algorithm from the MPP locus. The flowchart is presented by Fig. 3. It starts by climbing the *P–V* curve until it reaches the vicinity of MPP. Similar to the other P&O, the operating point (V^*_{MPP}) oscillate around MPP. However, the oscillation is detected by a special mechanism (that shall be described later) and the perturbation size is reduced until it reaches a certain minimum value. A very small power tolerance is allowed to handle tiny flickers as a result of circuit noise and small deviation of the irradiance.

Due to the small oscillation, there will be always a difference in power (ΔP) at every consecutive sample. The value of $\Delta P/P$ (the normalized power change) is kept below a certain threshold limit (T_{r1}) because the perturbation size has reached its minimum value. If $\Delta P/P > T_{r1}$, it implies that the irradiance is changing (either ascending or descending). In the real environment, the irradiance varies in three possible ways: (1) slow-gradual (0.1–5 W/m^2/s), (2) fast–gradual (>5 W/m^2/s) and (3) rapid (step) change. These possibilities are illustrated in Fig. 4. For the gradual changes (both slow and fast), the power increases or decreases in tandem with the change in the irradiance. On the other hand, rapid change constitutes a step change in the irradiance. To determine whether the change in irradiance is gradual or rapid, another threshold value (T_{r2}) is introduced. If $T_{r1} < \Delta P/P < T_{r2}$, the change in the irradiance is considered as gradual. In this case, the perturbation size is increased. However, under this circumstance, there are possibilities that the divergence from the MPP locus can occur. To prevent this from happening, a boundary condition is imposed to restrain the V^*_{MPP} within the range of the MPP locus. Ultimately, the change in irradiance stops; the oscillation is detected and the perturbation size will be reduced to the minimum again. On the other hand, if $\Delta P/P > T_{r2}$, the irradiance is considered to change rapidly from one level to the next (step). In such case, it is sufficient to increase the perturbation size to ensure that the MPP is tracked at a new level of irradiance.

3.2. Setting of the initial points

The initial voltage (V^*_{MPP}) is set to 65% of V_{oc}, where V_{oc} is the open circuit voltage of the PV array. The slope is determined in a similar way to conventional P&O, i.e. using the signs of ΔP and ΔV. The "value" of the slope is the sign multiplication of these two quantities and normalized to unity, as shown in Table 1.

The detection of oscillation is done by the recording three consecutive slope values. When voltage is increasing, the sign of the slope is positive, and vice versa. Thus, during the increase or decrease of the voltage, the three consecutive sign of slope will be either positive or negative. Thus the absolute value of the summation of the slope value will be 3. After reaching at the MPP when oscillation starts, operating point will move two times in one direction and then move to the opposite direction. As a result under continuous oscillation three consecutive sign of slope will never be same. It will be a combination of positive and negative values. Thus, the absolute summation of the slope value will be less than 3. Thus the following inequality can be derived:

$$if \sum slope = \begin{cases} 3 & \text{MPPT not converged to steady state} \\ < 3 & \text{MPPT converged to steady state} \end{cases} \quad (4)$$

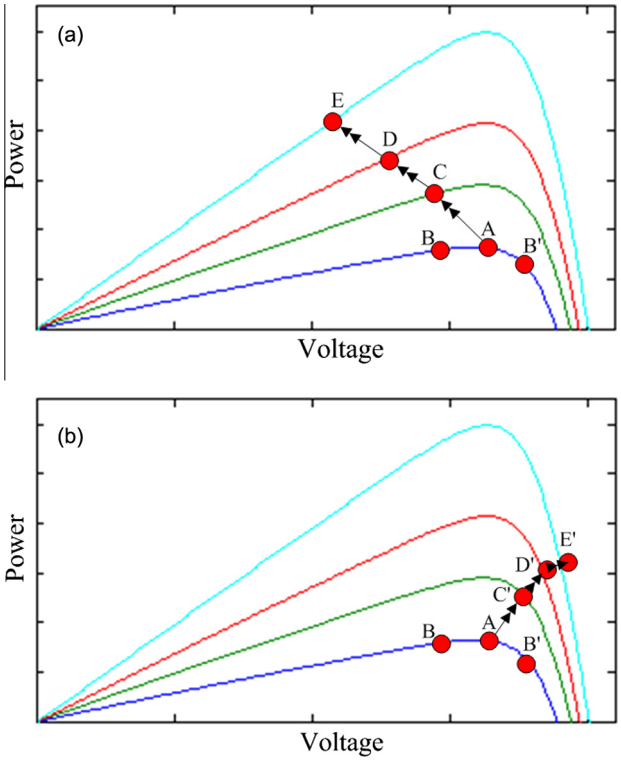

Fig. 2. Losing the tracking direction by P&O (a) towards left and (b) towards right side of MPP.

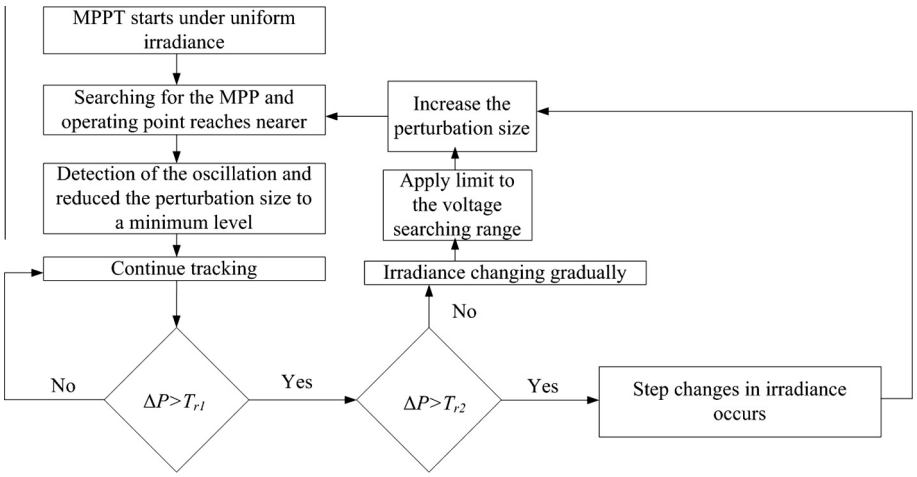

Fig. 3. General outline of the proposed P&O algorithm.

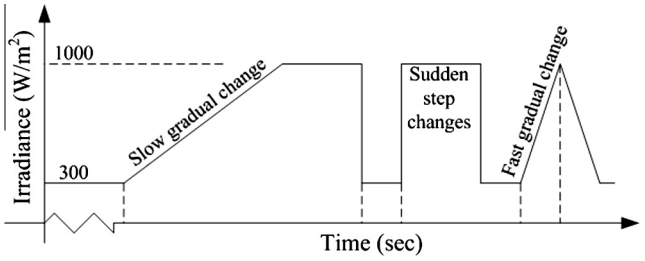

Fig. 4. Different types of irradiance change.

The initial perturbation size is set to $\phi = 2\%$ of V_{oc} [24]. As the operating point converges near to MPP, the oscillation is detected by Eq. (4). Then the size of the perturbation is reduced by 0.5% of V_{oc} for every iteration step. The perturbation size is continuously reduced until it reaches 0.5% of V_{oc}. The tiny oscillation will result almost zero power loss and at the same time immunize the algorithm from very small changes of the irradiance and the noise in the circuits.

3.3. Change of irradiance and setting the boundary condition

For the proposed P&O scheme, as operating point converges to MPP, the perturbation size becomes very small; thus it is able to handle slow-gradual change in the irradiance easily. However, when irradiance changes at a faster rate, it may lose the tracking direction. To avoid this, a flag is introduced. Initially, the flag is low, but once the oscillation is detected, it is toggled to high. This flag remains high until $\Delta P/P > T_{r1}$. Then the second threshold value, i.e. T_{r2}, is checked. If $T_{r1} < \Delta P/P < T_2$, it implies that the change of power is small; thus a gradual change in irradiance is occurring. In this case, the perturbation size is restored to 2% of V_{oc}. Additionally, since the gradual change occurs; the voltage boundary condition is imposed. The value of the boundaries values are estimated as follows. The initial voltage boundaries are set, i.e. 0 to V_{oc}. When the flag is high, the boundaries are changed to (V^*_{MPP}-5% of V_{oc}) and (V^*_{MPP}+ 5% of V_{oc}). These values are selected because when the irradiance decreases, the position of the V_{MPP} shifts slightly to the left. The shifting is observed to be approximately 5% of the V_{oc}. This is demonstrated by Fig. 5. Thus by applying the 5% margin, the MPPT is forced to remain near the MPP during gradual irradiance change—thus avoiding the loss of tracking condition.

Table 1
Determination of the slope "value".

Sign of ΔP	Sign of ΔV	Slope value
Positive	Positive	+1
Positive	Negative	−1
Negative	Positive	−1
Negative	Negative	+1

It is reported in [25], under normal condition, the maximum irradiance change can be 0.027 KW/m^2/s. Thus the maximum gradual occurrence of $\Delta P/P$ can be 0.027. To make the algorithm more robust, T_{r1} and T_{r2} are chosen to be 0.001 (lower than 0.027) and 0.05 (higher than 0.027), respectively. Thus, any irradiance change in between 1.0 W/m^2/s to 50 W/m^2/s is considered as the gradual change. A value higher than 50 W/m^2/s is detected as the step change. In case of the step changes, the perturbation size is increased to 2% of V_{oc}. However, the voltage boundaries are not imposed because MPP divergence is not relevant for the step change in irradiance.

4. Implementation

4.1. PV modeling

To simulate the PV system, the multiple string two-diode model [26], as shown in Fig. 6 is utilized. Variable N_S is the number of modules per string, while N_P indicates the number of string in the array. If N is N_S/N_P, the PV current drawn from the system can be written as

$$\begin{aligned} I &= I_{PV}N_p - I_{D1} \\ &= I_{d1}N_p\left[\exp\left(\frac{V+NIR_s}{a_1V_{T1}N_s}\right)\right] - I_{d2}N_p\left[\exp\left(\frac{V+NIR_s}{a_2V_{T2}N_s}\right)\right] \\ &\quad - \frac{V+NIR_s}{NR_p} \end{aligned} \tag{5}$$

where I and V are the PV current and voltage, respectively; R_s is the series, while R_p is the parallel resistance; $V_{T1} = V_{T2}$ is the thermal voltage of the diodes. The light generated current (I_{PV}) is given by

$$I_{PV} = (I_{PV\_STC} + K_I(T - T_{STC}))\frac{G}{G_{STC}} \tag{6}$$

Note that I_{PV_STC} is measured in the standard test condition (STC),[1] Variable K_I is the short circuit current coefficient, which is usually provided by the manufacturer. The diode saturation current is given by

[1] At STC, temperature $T = 298$ K and irradiance $G = 1000$ W/m^2.

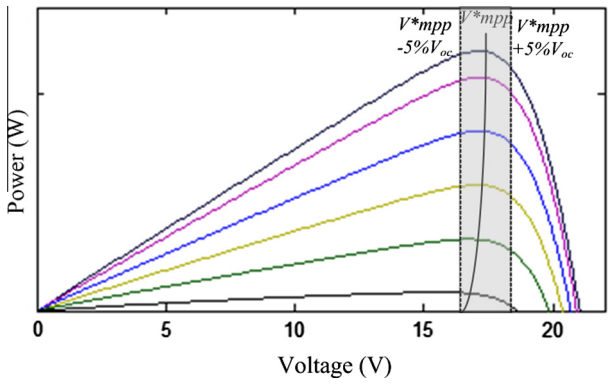

Fig. 5. The position change of V_{mpp} depending of the irradiance level.

$$I_{d1} = I_{d2} = \frac{I_{SC\_STC} + K_I(T - T_{STC})}{\exp((V_{OC\_STC} + K_V(T - T_{STC}))/V_T) - 1} \quad (7)$$

In Eq. (5), I_{SC_STC} and V_{OC_STC} are the short circuit current and the open circuit voltage in STC, respectively. Variable K_V is the open circuit voltage coefficients. The specifications for the PV module used in this paper are given in Table 2. Using these parameters, the corresponding *P–V* and *I–V* curves for the variation in irradiance and temperature are plotted in Figs. 7(a) and (b), respectively. Each curve presents its unique maximum power point (MPP) location.

4.2. Experimental set-up

Fig. 8 presents the MATLAB simulation model for the overall PV system. The P&O algorithm is realized using a buck-boost converter. This converter is selected to its suitability for MPPT problem, as suggested by various authors, for example [27]. The buck-boost is designed to operate in the continuous inductor current mode, with the specifications shown in Table 3.

The PV model described in Section 4.1 is labeled as "PV Array" block in Fig. 8. Its inputs are the *G* and *T*. These are profiles of irradiance and temperature that will be imported using look-up tables. The outputs are the PV voltage (V_{PV}) and current (I_{PV}). They measured using voltage and current sensor. Multiplying these two quantities gives the present value of power. This value is fed to the MPPT block, which in turn will return the value of V_{out} (V^*_{MPP}). An error voltage (V_{error}) is obtained by subtracting V_{ref} (V_{PV}) from the V_{out}, which is then fed to a proportional–integral (PI) controller. The output of the PI controller is compared to a sawtooth waveform to produce the duty cycle (*D*) for the converter. The converter is forced to operate using this value of *D*, which results desired

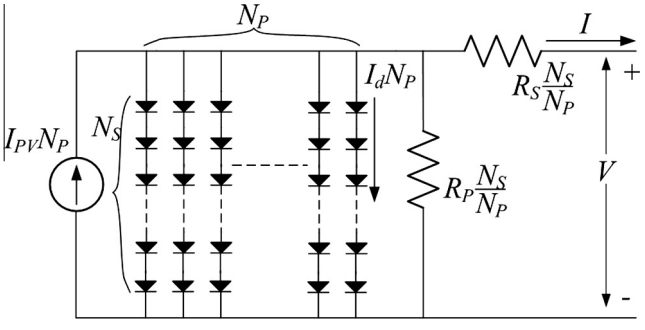

Fig. 6. The two-diode model of PV cell that is used throughout this paper.

Table 2
The specifications of the PV module.

Parameters	Variable	Value	Unit
Short circuit current	I_{SC}	3.8	A
Open circuit voltage	V_{OC}	21.1	V
Current at Pmax	I_{MPP}	3.5	A
Voltage at Pmax	V_{MPP}	17.1	V
Maximum power	P_{MPP}	59.85	W
V_{OC} coef. of temperature	K_V	−0.08	V/°C
I_{SC} coef. of temperature	K_I	$3e^{-3}$	A/°C
No. of modules in series (per string)	N_S	10	–
No. of parallel strings	N_P	2	–

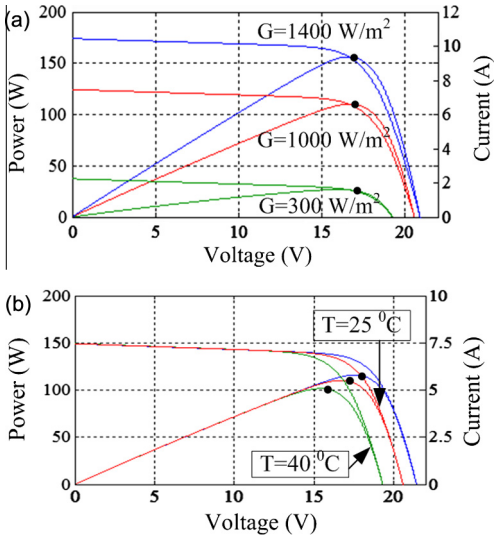

Fig. 7. The *I–V and P–V* curves for two modules in parallel with specifications given in Table 2. (a) under varying solar irradiance. (b) under varying temperature.

voltage, i.e. V^*_{MPP}. The best values of the PI controller are tuned by trial and error method and are shown in Table 3.

4.3. Performance benchmarking

The effectiveness of the proposed P&O algorithm is measured by its MPPT efficiency. The instantaneous MPPT efficiency is which is computed by the following formula:

$$\eta_{MPPT} = \frac{P_{MPP}(t)}{P_{MPP*}(t)} \times 100 \quad (8)$$

The average MPPT efficiency is given as

$$\eta_{MPPT(avg)} = \frac{\int P_{MPP}(t)dt}{\int P_{MPP*}(t)dt} \times 100 \quad (9)$$

In Eqs. (8) and (9), P_{MPP*} is the maximum theoretical power that can be achieved, which is the target of the algorithm. It is computed using the PV model. On the other hand, P_{MPP} is the actual power that is extracted using the MPPT algorithm. It depends on how close the algorithm tracks the irradiance at any instant of time. To calculate P_{MPP}, the measured values of V_{PV} and I_{PV} are required.

The performance of the conventional, adaptive and proposed P&O is benchmarked using three tests, namely (1) Ropp (2) sinusoidal and (3) ramp irradiance. In addition, to establish how these algorithms perform under real environmental condition, they are subjected to a one-day irradiance and temperature profile. For the adaptive P&O, the logarithmic scheme [18] is used.

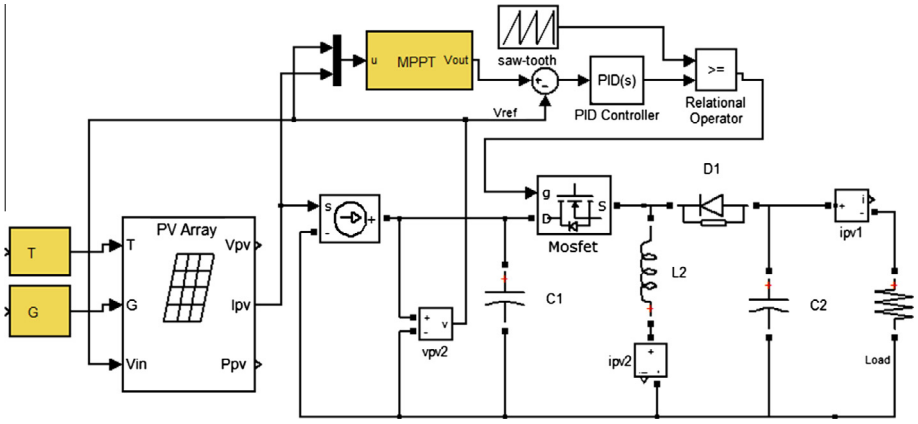

Fig. 8. The buck boost circuit used to implement the MPPT.

Table 3
Specifications for the buck-boost converter.

Component/parameter	Label	Value
Switching frequency	f	100 kHz
Buck-boost inductor	L	1 mH
Buck-boost capacitor	C_2	470 μF
Input capacitor	C_1	470 μF
Proportional constant (P)	P	0.08
Integral constant (I)	I	15

5. Results and discussions

5.1. The Ropp test

The Ropp test was originally proposed by [19]—using an irradiance profile shown in the Fig. 9(a). The test determines if the MPPT algorithm is able to cope with the gradual as well as sudden step changes of the irradiance. In addition, it also includes the steady-state condition. The profile starts at 200 W/m^2. During the initial ascend (60–140 s), the irradiance increases gradually from 200 to 1000 W/m^2. Then four step changes are made: (1000–200), (200–600), (600–200) and (200–1000) W/m^2. Finally irradiance descends gradually from 1000 to 200 W/m^2.

The tracking performances of conventional and proposed P&O based MPPT can be determined from the output power plot shown in Fig. 9(b). For the conventional P&O, the perturbation size is fixed at 2% of V_{oc}. As can be observed, the proposed P&O tracks the irradiance profile almost perfectly. The amplitude of oscillation is very low and it never loses its tracking locus. On the other hand, the conventional P&O exhibits large oscillation at steady state as shown by the inset (zoomed portion) of the figure. Furthermore, during the gradual ascending of the irradiance, the conventional P&O lost its tracking direction numerous times. However, during the descends of irradiance, no loss of tracking is observed. This is consistent with the explanation given in Section 2.2. The comparison between the adaptive and proposed P&O is illustrated in Fig. 9(c). It can be seen, the adaptive P&O still loses the tracking direction at several points; an example is shown by the enlarged image. Furthermore, during steady state, it keeps on oscillating, even though the perturbation size is very small. As a result, the tracked power is slightly below the actual MPP.

Fig. 10(a), (b) and (c) shows the MPPT efficiency (η_{MPPT}) as computed by Eq. (8). Due to the oscillation, the η_{MPPT} of the conventional P&O varies in the range of 95–99.5%. However, during the loss of tracking direction, the η_{MPPT} drops to as low as 75%. In the case of adaptive P&O, the efficiency is maintained around 99% for most of the time. However during the tracking divergence, the efficiency falls to the 90% region. For the proposed P&O, the steady state oscillation is extremely small. Furthermore, during the change of irradiance—unlike the conventional and adaptive P&O, it is able to follow the power locus very closely. This is the results of the effective control of the boundary conditions, as explained in Section 3.2. However, when the steady state condition is detected, it very quickly reduces the perturbation size to avoid large oscillations. The computed average MPPT efficiency, i.e. $\eta_{MPPT(ave)}$ over the total Ropp profile cycle for the conventional, adaptive and proposed version is 97.52%, 98.84% and 99.4%, respectively.

5.2. Sine irradiance

In the Ropp test, although the irradiance profile is highly dynamic, the rise or fall of the slopes is linear. This is not necessary true in the real environmental conditions. To represent for the non-linear slopes, another test named as the sinusoidal irradiance is developed. Its objective is to determine whether the MPPT algorithm is able to track an irradiance profile with varying irradiance rate at every sampling time. Fig. 11(a) depicts the profile for the sinusoidal test. It begins at 800 W/m^2. Similar to the Ropp test, a 5 s dwelling time provided. Then irradiance starts to vary between 600 W/m^2 and 1000 W/m^2, according to the change in the sinusoidal curve.

The tracking performance of the conventional and the proposed P&O is illustrated in Fig. 11(b). As can be observed in the enlarged image, as the irradiance increases, the conventional P&O repeatedly loses the tracking direction. As a result, its efficiency drops for brief periods, as depicted by the Fig. 12(b). In the case of adaptive P&O, an interesting situation occurs during the positive rise of the sine wave, i.e. between 8 and 12 s. As can be seen in Fig. 11(c), the algorithm is not able to maintain the tracking, particularly when irradiance gradually increased at a higher rate. The reason is that, when the perturbation size becoming smaller (as it reaches the steady state), it could not cope with the larger change in the irradiance. In such condition, what the algorithm needs is the contrary, i.e. larger perturbation size. As a result of the insufficient perturbation size, the voltage drops and it loses the track of the MPP. On the other hand, the proposed P&O tracks the power locus quite with near perfection. The only departure from the reference occurs when the operating point reaches the peaks and valleys of the sinusoidal. This happens due to the fact that when the irradiance is descending, the MPP voltage shifts slightly to the left. Since the sinusoidal waveform is continuously changing, the operating point is not given an opportunity to settle at a new MPP for a while, unlike the Ropp test. As a result, the efficiency drops slightly around these points.

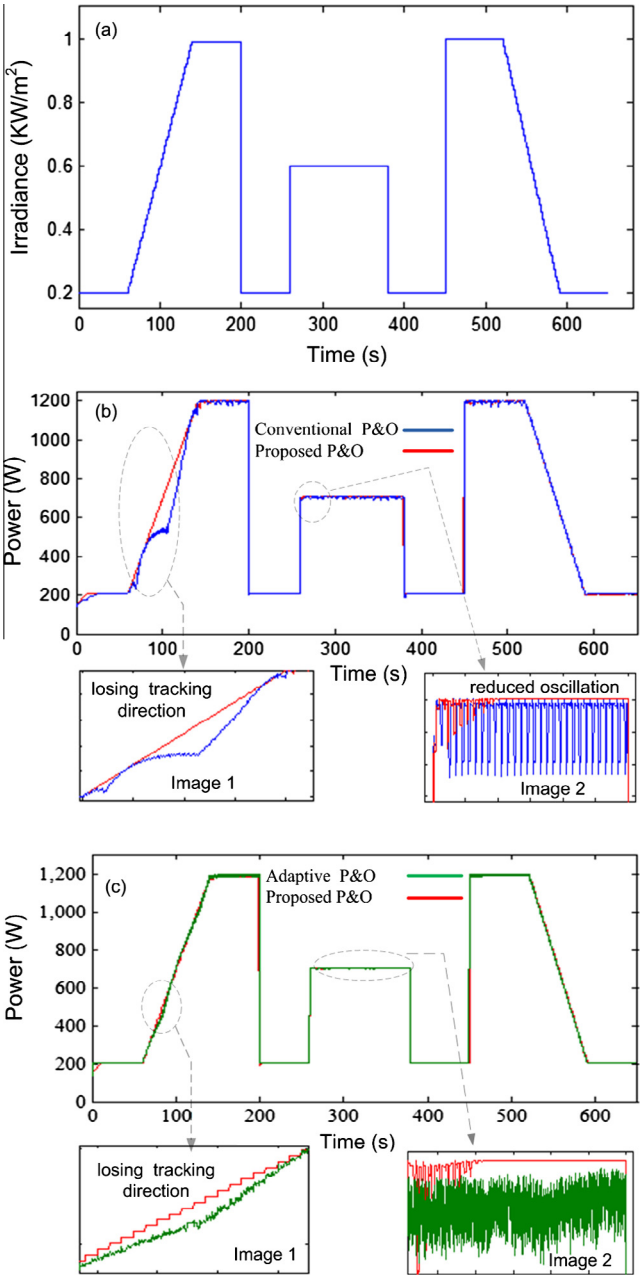

Fig. 9. (a) Irradiance profile for the Ropp test (b) Comparison of the tracking performance of the conventional P&O and proposed P&O. (c) Tracking performance of the adaptive P&O and proposed P&O.

Due to the repeated loss of the tracking direction, the $\eta_{MPPT(ave)}$ for the conventional P&O dropped down to 98.3%. In several cases, the instantaneous efficiency goes as low as 95%. In the case of adaptive P&O, the large drop during the gradual change in irradiance causes $\eta_{MPPT(ave)}$ to be in the range of 98%. On the other hand the proposed P&O exhibits excellent tracking over the whole test curve. Its instantaneous efficiency is continuously above 99.5% under all conditions, while the $\eta_{MPPT(ave}$ is approximately 99.8%. The efficiency profiles for all cases are shown in Fig. 12(a)–(c).

5.3. The ramp irradiance

The objective of the ramp test is to quantify the ability of the MPPT to track ascending and descending irradiance triangle with various slopes values. A total of seven ramps are utilized, with gradients from 5.0 W/m^2/s to 50 W/m^2/s. Thus, it covers a comprehensive range of irradiance change profile, i.e. from a slow to very fast (almost step change). At the peak and valley of each ramp, a small dwell time (0.5 s) is given to allow for the operating point to settle at a particular MPP, before ascending or descending again. The full irradiance profile of the test is shown in Fig. 13(a).

The tracking performance of the conventional and proposed P&O is presented in Fig. 13(b). During the slow irradiance change, i.e. ramp No. 1, the proposed P&O tracks the power locus almost perfectly. This is illustrated by the inset, i.e. image 1. On the other hand, as expected, the conventional P&O exhibits steady state oscillation. There is also an occasion whereby it diverges from its intended power locus. As the slope of the ramp is increased, it loses the tracking direction more frequently. These are depicted in the images 2, 3 and 4, respectively. In image 4, (50 W/m^2/s) the algorithm almost fail to reach the peak value of the ramp. For the adaptive P&O, it tracks the initial ramps quite successfully. As the gradient of the ramp increases, it loses the tracking direction occasionally. However, the occurrence is not as frequent as the conventional P&O. Nevertheless, the reduction in the power yield is significant. Furthermore, it can be seen from the enlarged images in Fig. 13(c) that it failed to reach the peaks of the ramps with gradients 20, 30 and 50 W/m^2/s.

The steady state oscillation and tracking divergence is reflected in the efficiency. Fig. 14(a) shows the efficiency profile for the conventional P&O. As can be observed, the efficiency drops significantly during tracking divergence. Additionally, the drop is also

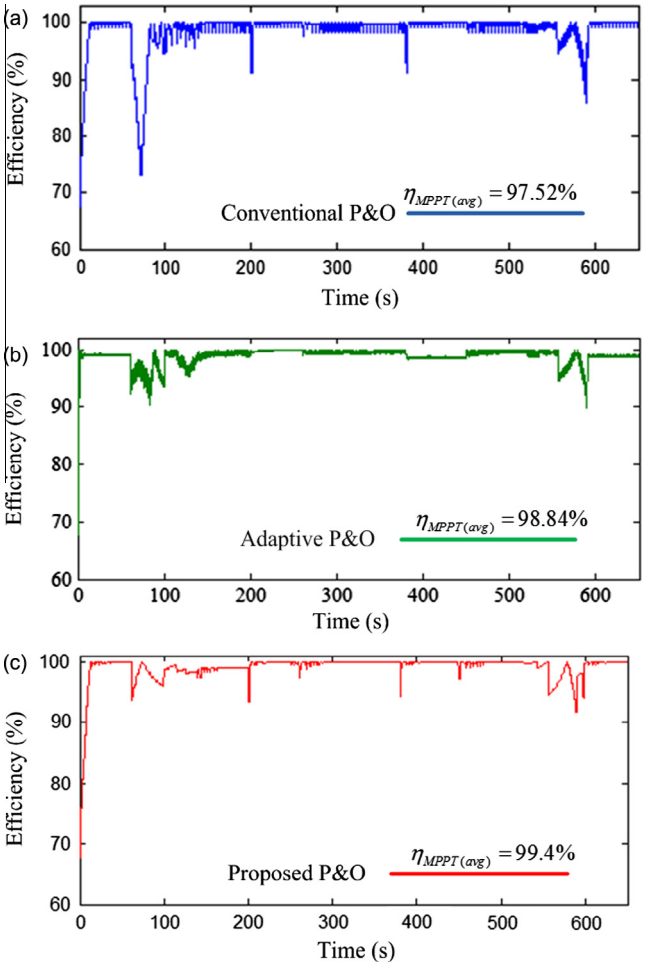

Fig. 10. Efficiency profile of (a) conventional P&O (b) adaptive P&O (f) proposed P&O.

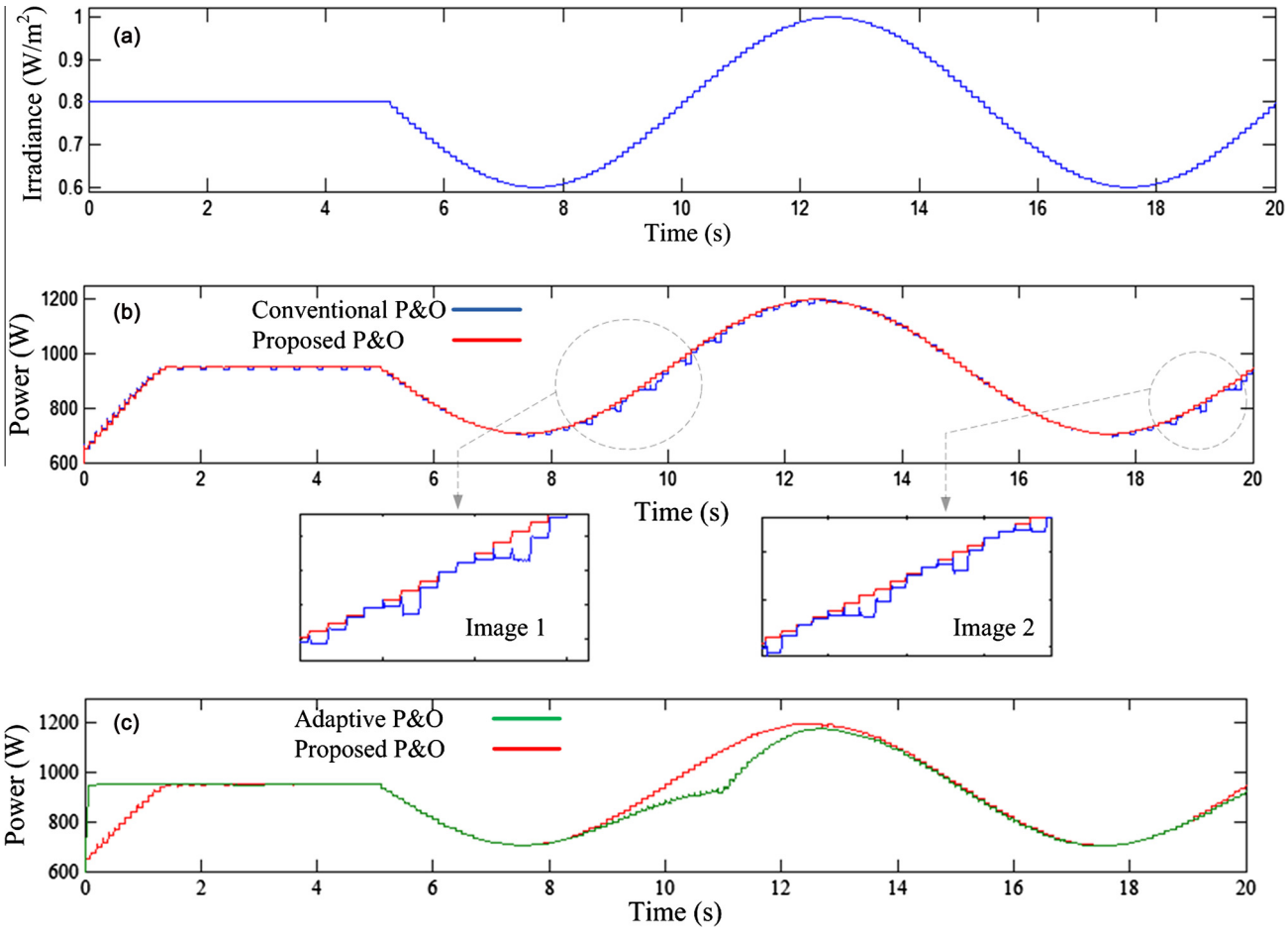

Fig. 11. (a) Irradiance profile for the sinusoidal irradiance test. (b) Comparison of tracking performance between the conventional P&O and proposed P&O (c) Comparison of tracking performance between the adaptive P&O and proposed P&O.

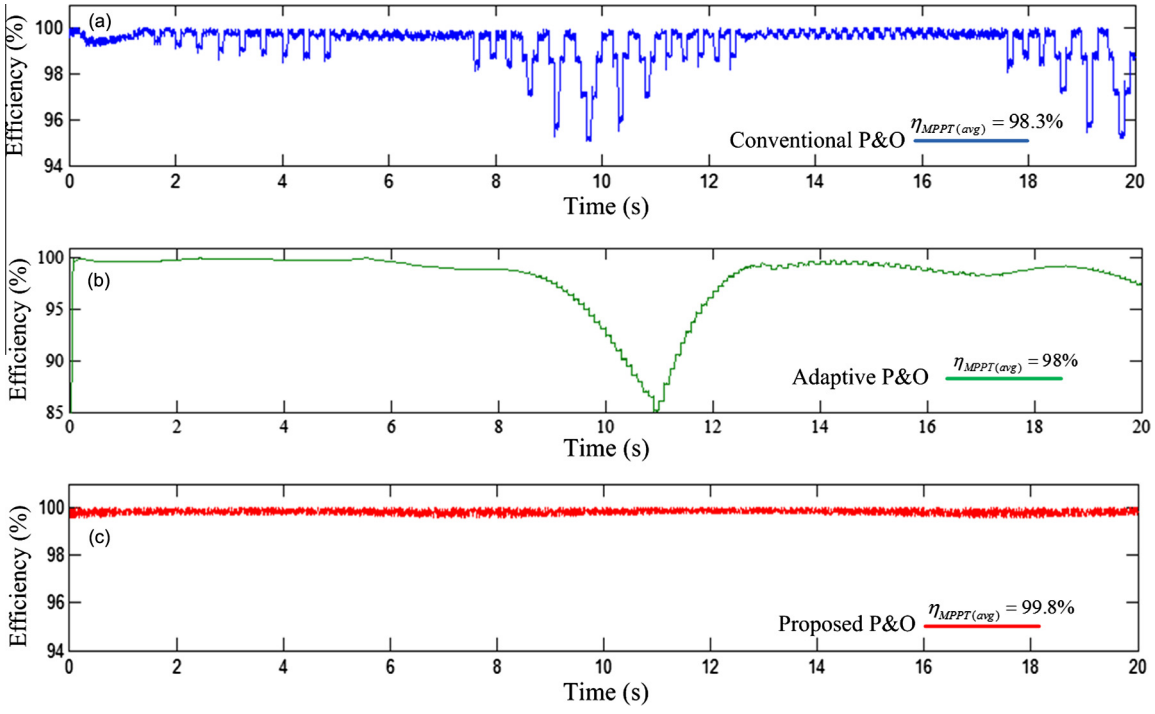

Fig. 12. Efficiency profile of the (a) conventional P&O (b) adaptive P&O (c) proposed P&O.

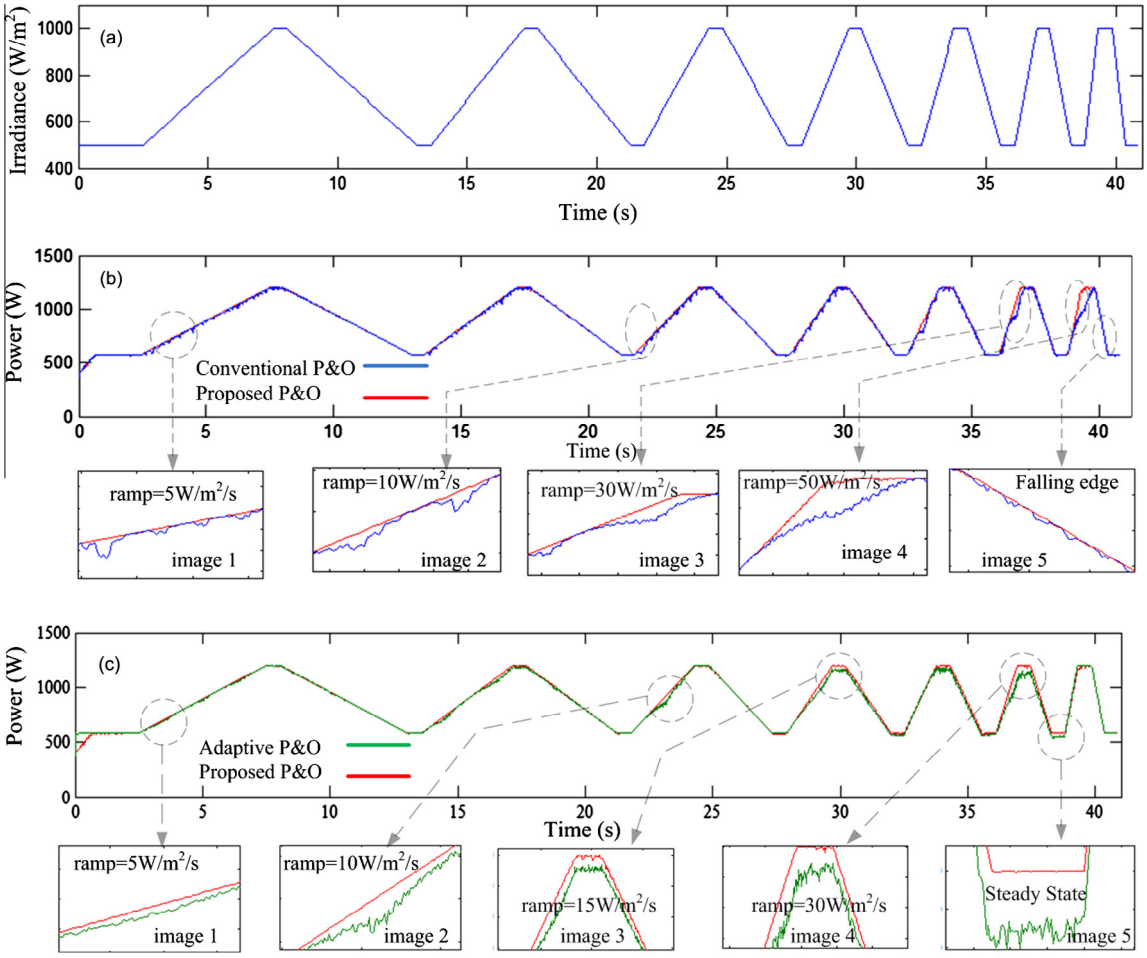

Fig. 13. (a) Ramp irradiance profile (b) Tracking performance of the conventional P&O and proposed P&O. (c) Tracking performance of the adaptive P&O and proposed P&O.

contributed by the steady state oscillation. Its average efficiency, ($\eta_{MPPT(avg)}$) is approximately 96.5%. However, as can be observed, for certain parts of the profile, the efficiency dips well below 90%. The efficiency profile for the adaptive P&O is shown in Fig. 14(b). The $\eta_{MPPT(avg)}$ is 97.5%. The efficiency plot for the proposed P&O is shown in Fig. 14(c). As can be seen, the η_{MPPT} is almost uniform throughout the irradiance profile. It recorded an $\eta_{MPPT(avg)}$ of almost 99.5%.

5.4. One-day irradiance and temperature profile

The MPPT techniques are subjected to a daily (ten-hour) irradiance and temperature profile as shown in Fig. 15 (a). This is a plotted using a meteorological data of a typical tropical day that includes the presence of intermittent clouds and occasional showers. The irradiance and temperature increase almost linearly since morning until midday. During the afternoon, irradiance remains almost constant with the sporadic occurrence of clouds and rain. As it approaches evening, the irradiance and temperature gradually falls.

The output power harvested by the conventional and proposed P&O is illustrated in Fig. 15(b). Since the traces for both are almost indistinguishable, four enlarged snapshots (images) are presented. Image 1 focus on the responses for the sudden increase in the irradiance increases (5 W/m^2/s). As can be seen, the conventional P&O loses the tracking continuously. On the other hand, the proposed P&O track the power locus almost perfectly. In image 2, a similar case is presented; the conventional P&O diverges from the MPP more frequently due to the higher rate of change in the irradiance (10 W/m^2/s). During the steady-state condition, (image 3), the conventional P&O maintains its tracking direction. However, the power oscillates continuously due to the fixed perturbation size. Image 4 represents the condition in which the irradiance descends gradually. During this interval, as explained, both the conventional and proposed P&O do not diverge from the MPP. However, the steady sate oscillation of the conventional P&O still persists. In Fig. 15(c) the adaptive and proposed P&O is compared. For clarity, four sections of the profile are zoomed. In these four images, it can be seen that the adaptive P&O is prone to lose the tracking due to the small perturbation sizes. On the contrary the proposed P&O detects the steady state almost perfectly and reduces the oscillation to the minimum level.

The efficiency of the conventional, the adaptive and the proposed P&O is presented in Figs. 16(a), (b) and (c), respectively. The measured $\eta_{MPPT(avg)}$ for the conventional P&O is approximately 97.5%. In certain cases the η_{MPPT} drops below 85% due of the loss of tracking direction. For the adaptive P&O $\eta_{MPPT(avg)}$ is 98.76%. Though it drops near to 95% occasionally, most of the time it is well above 97%. On the other hand, $\eta_{MPPT(avg)}$ for the proposed P&O is calculated at 99.2%. At most times, its efficiency is maintained well above 99%, except for the lower irradiance region, where it dips to near 97%. On the overall, the proposed P&O increases the $\eta_{MPPT(avg)}$ by 1.7%.

To conclude all tests carried, a summary of the performance are tabulated on Table 4. It can be deduced that, in general, the proposed P&O offers an increases in the average efficiency of

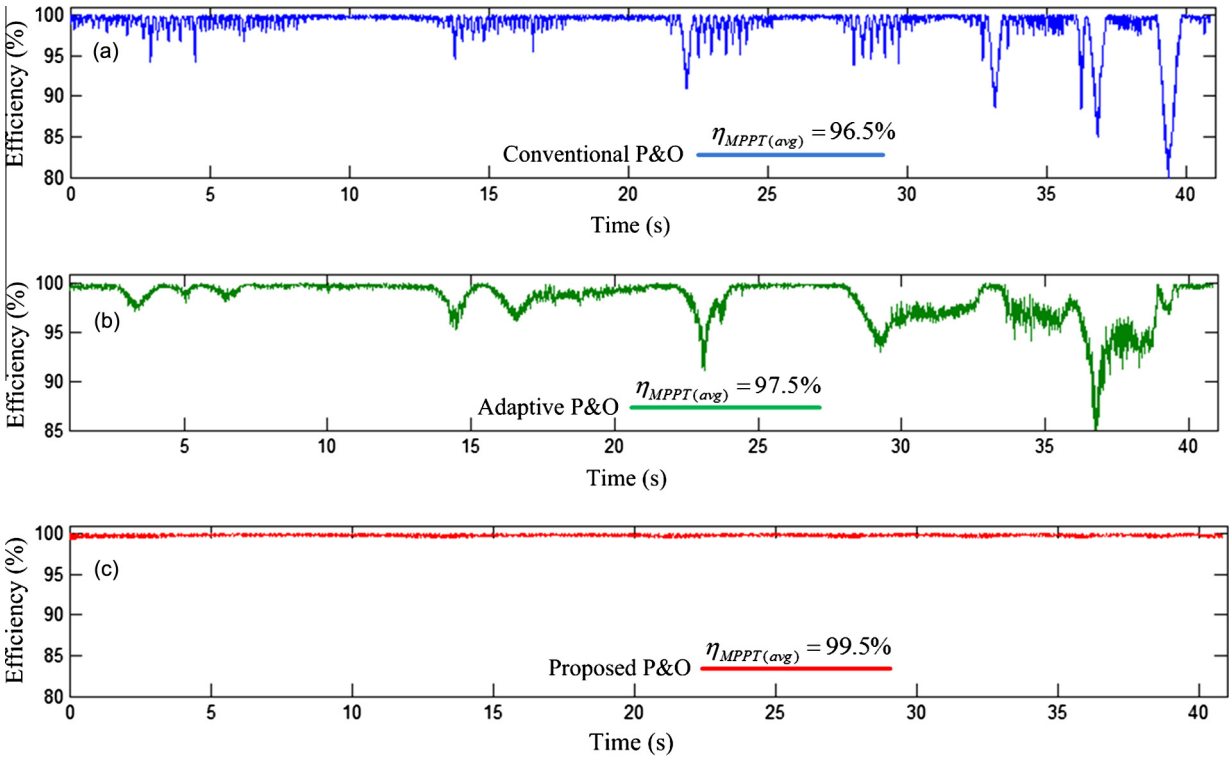

Fig. 14. Efficiency profile of (a) conventional P&O (b) adaptive P&O (c) proposed P&O.

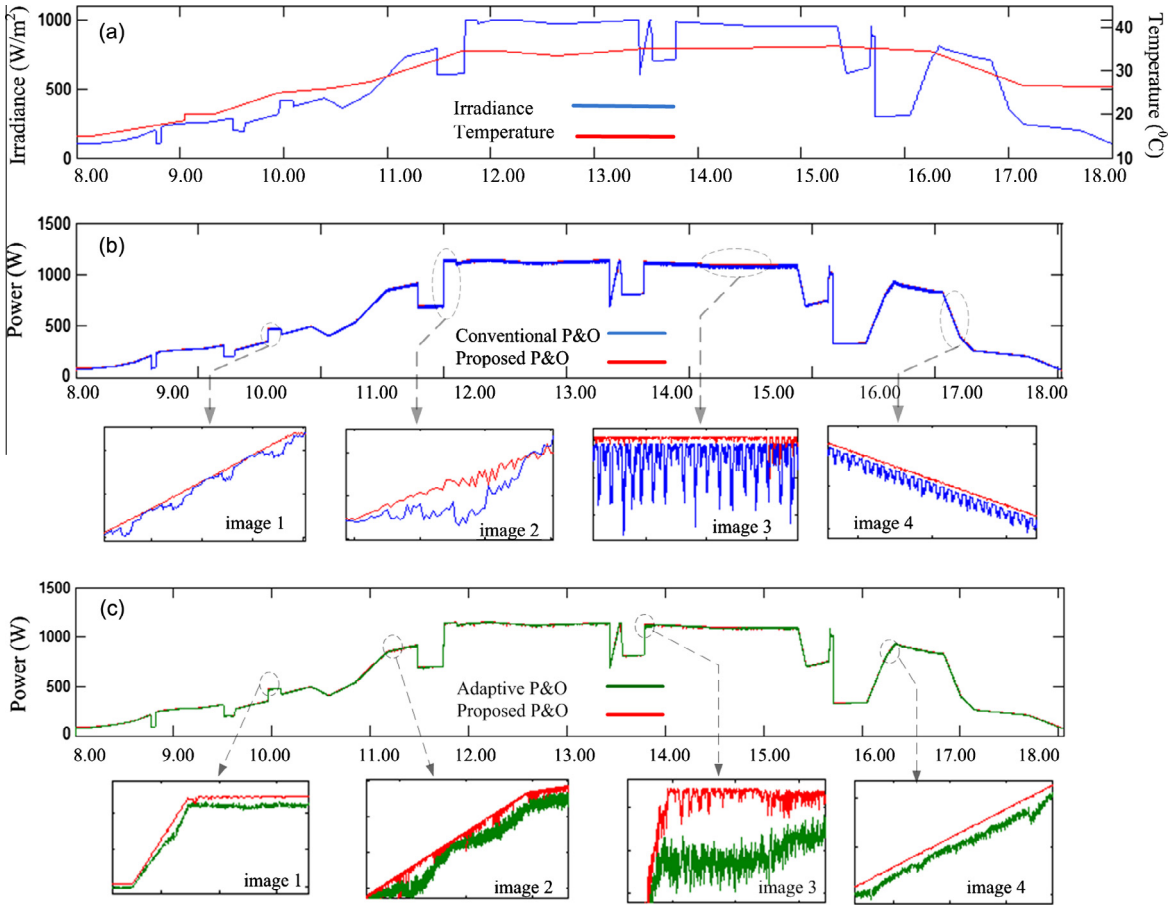

Fig. 15. (a) Daily irradiance profile (b) Tracking performance of the conventional P&O and proposed P&O. (c) Tracking performance of the adaptive P&O and proposed P&O.

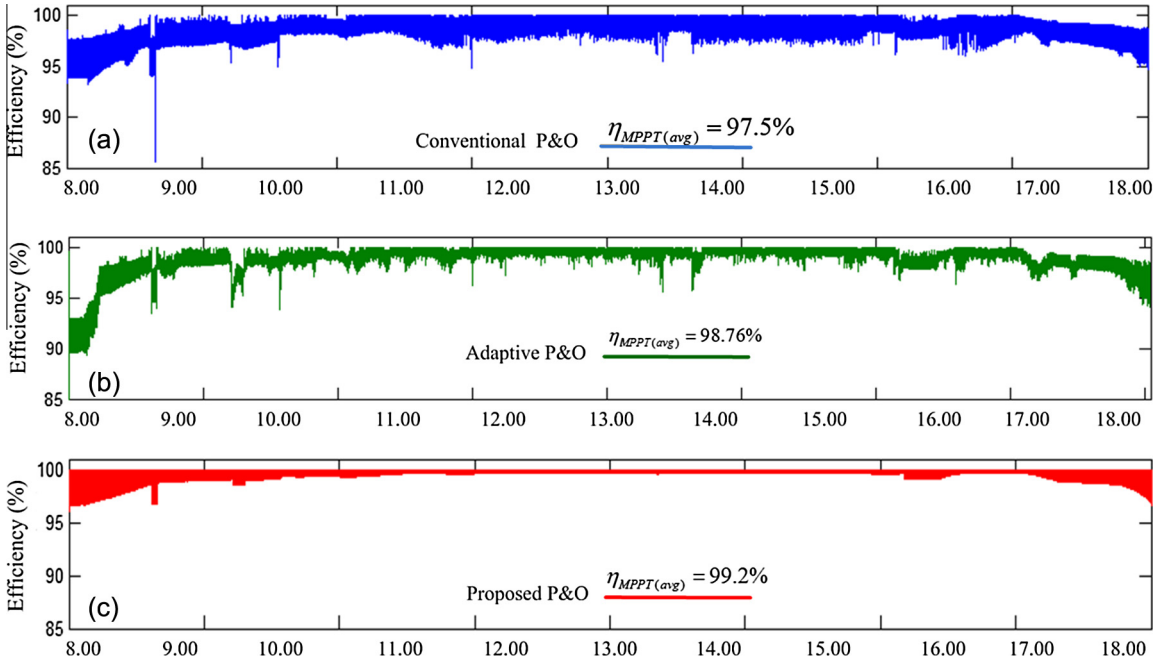

Fig. 16. Efficiency of (a) the conventional P&O (b) the adaptive P&O (c) the proposed P&O.

Table 4
Summary of MPPT efficiency (η_{MPPT}) for all tests.

Test type	Max efficiency (%)			Min efficiency (%)			Avg. efficiency (%)		
	Conventional	Adaptive	Proposed	Conventional	Adaptive	Proposed	Conventional	Adaptive	Proposed
Ropp	99.65	99.80	99.88	72.65	91.50	97.30	97.52	98.84	99.45
Sinusoidal	99.65	99.70	99.93	95.42	85.70	99.58	98.30	98.00	99.82
Ramp	99.65	99.60	99.93	80.03	85.50	99.42	96.45	97.5	99.55
One day profile	99.65	99.70	99.82	86.49	90.50	96.55	97.51	98.76	99.20

approximately two percentage points. For a PV system, this improvement is very significant due to the fact that an installed system has a life-time of approximately twenty years. Based on this observation, there is a strong justification to consider its application over the conventional and adaptive P&O. Besides, the proposed algorithm does not require additional hardware; only a handful line of software codes need to be embedded into the MPPT control program.

6. Conclusion

A scheme to improve the efficiency of the P&O MPPT has been described. It reduces the steady state oscillation and eliminates the probability of divergence form the MPP locus. The proposed method is evaluated against the conventional and adaptive P&O based MPPT by using the Ropp, sinusoidal and ramp irradiance tests. In addition, these are subjected to a one-day (10 h) irradiance and temperature profile. In all the cases, the proposed method outperforms the conventional and the adaptive P&O. It was found that, for all the tests, the η_{MPPT} of the proposed P&O increases by approximately two percentage points. This improvement is important since a PV installation has a life-time of approximately twenty years. Since there proposed version maintains the similar algorithm structure with the conventional, the former can be easily implementable with a low-cost microcontroller, similar to the conventional one.

Acknowledgments

The authors would like to thank Universiti Teknologi Malaysia and the Ministry of Higher Education, Malaysia for providing the facilities and financial support (Research University Grant No. Q.J130000.2509.06H78) to conduct this research.

References

[1] Rehman S, Bader MA, Al-Moallem SA. Cost of solar energy generated using PV panels. Renew Sustain Energy Rev 2007;11:1843–57.
[2] Wei H, Liu J, Yang B. Cost-benefit comparison between Domestic Solar Water Heater (DSHW) and Building Integrated Photovoltaic (BIPV) systems for households in urban China. Appl Energy 2014;126:47–55.
[3] Krebs FC. Fabrication and processing of polymer solar cells: a review of printing and coating techniques. Sol Energy Mater Sol Cells 2009;93:394–412.
[4] Zhang W, Zhu R, Liu B, Ramakrishna S. High-performance hybrid solar cells employing metal-free organic dye modified TiO2 as photoelectrode. Appl Energy 2012;90:305–8.
[5] Ishaque K, Salam Z. A review of maximum power point tracking techniques of PV system for uniform insolation and partial shading condition. Renew Sustain Energy Rev 2013;19:475–88.
[6] Ahmed J, Salam Z. A Maximum Power Point Tracking (MPPT) for PV system using Cuckoo Search with partial shading capability. Appl Energy 2014;119:118–30.
[7] Ramli MZ, Salam Z. A simple energy recovery scheme to harvest the energy from shaded photovoltaic modules during partial shading. Power Electron, IEEE Trans 2014;29:6458–71.
[8] Salam Z, Ahmed J, Merugu BS. The application of soft computing methods for MPPT of PV system: a technological and status review. Appl Energy 2013;107:135–48.

[9] Esram T, Chapman PL. Comparison of photovoltaic array maximum power point tracking techniques. Energy Conversion, IEEE Trans 2007;22:439–49.
[10] Piegari L, Rizzo R. Adaptive perturb and observe algorithm for photovoltaic maximum power point tracking. Renew Power Generation, IET 2010;4:317–28.
[11] Mamarelis E, Petrone G, Spagnuolo G. A two-steps algorithm improving the P&O steady state MPPT efficiency. Appl Energy 2014;113:414–21.
[12] Alonso R, Ibaez P, Martinez V, Roman E, Sanz A. An innovative perturb, observe and check algorithm for partially shaded PV systems. Power Electronics and Applications, 2009 EPE '09 13th European Conference on 2009. p. 1–8.
[13] Fermia N, Granozio D, Petrone G, Vitelli M. Predictive & adaptive MPPT perturb and observe method. Aerospace Electron Syst, IEEE Trans 2007;43:934–50.
[14] Femia N, Petrone G, Spagnuolo G, Vitelli M. Optimization of perturb and observe maximum power point tracking method. Power Electron, IEEE Trans 2005;20:963–73.
[15] Abdelsalam AK, Massoud AM, Ahmed S, Enjeti P. High-performance adaptive perturb and observe MPPT technique for photovoltaic-based microgrids. Power Electron, IEEE Trans 2011;26:1010–21.
[16] Yang Y, Zhao FP. Adaptive perturb and observe MPPT technique for grid-connected photovoltaic inverters. Procedia Eng 2011;23:468–73.
[17] Pradhan R, Subudhi B. Design and real-time implementation of a new auto-tuned adaptive MPPT control for a photovoltaic system. Int J Electr Power Energy Syst 2015;64:792–803.
[18] Zhang F, Thanapalan K, Procter A, Carr S, Maddy J. Adaptive hybrid maximum power point tracking method for a photovoltaic system. Energy Conversion, IEEE Trans 2013;28:353–60.
[19] Ropp M, Cale J, Mills-Price M, Scharf M, Hummel S. A test protocol to enable comparative evaluation of maximum power point trackers under both static and dynamic irradiance. Photovoltaic Specialists Conference (PVSC), 2011 37th IEEE: IEEE; 2011. p. 003734-7.
[20] Sera D, Teodorescu R, Hantschel J, Knoll M. Optimized Maximum Power Point Tracker for fast changing environmental conditions. Industrial Electronics, 2008 ISIE 2008 IEEE International Symposium on 2008. p. 2401–7.
[21] Zhang L, Al-Amoudi A, Bai Y. Real-time maximum power point tracking for grid-connected photovoltaic systems, 2000.
[22] Femia N, Petrone G, Spagnuolo G, Vitelli M. A technique for improving P&O MPPT performances of double-stage grid-connected photovoltaic systems. Ind Electron, IEEE Trans 2009;56:4473–82.
[23] Xiao W, Dunford WG. A modified adaptive hill climbing MPPT method for photovoltaic power systems. Power Electronics Specialists Conference, 2004 PESC 04 2004 IEEE 35th Annual: Ieee, 2004. p. 1957–63.
[24] Bennett T, Zilouchian A, Messenger R. A proposed maximum power point tracking algorithm based on a new testing standard. Sol Energy 2013;89:23–41.
[25] Bletterie B, Bruendlinger R, Spielauer S. Quantifying dynamic MPPT performance under realistic conditions first test results–The way forward. In: 21st European photovoltaic solar energy conference, Dresden, 2006.
[26] Ishaque K, Salam Z, Taheri H. Simple, fast and accurate two-diode model for photovoltaic modules. Sol Energy Mater Sol Cells 2011;95:586–94.
[27] Ishaque K, Salam Z, Amjad M, Mekhilef S. An improved particle swarm optimization (PSO)–based MPPT for PV with reduced steady-state oscillation. Power Electron, IEEE Trans 2012;27:3627–38.